Morris, J.D., Villinger, H.W., and Klaus, A. (Eds.)
Proceedings of the Ocean Drilling Program, Scientific Results Volume 205

2. Data Report: Barium Cycling at the Costa Rica Convergent Margin[1]

Evan A. Solomon,[2] Miriam Kastner,[2] and Gretchen Robertson[2]

ABSTRACT

Barium concentrations were measured on 17 pore fluid and 13 sediment samples from Sites 1253 and 1254 drilled offshore Costa Rica during Ocean Drilling Program (ODP) Leg 205. An additional 83 pore fluid and 29 sediment samples were analyzed for Ba concentrations from Sites 1039 and 1040 drilled during ODP Leg 170 offshore Costa Rica. Sites 1039/1253 and 1040/1254 are part of a transect across the Middle America Trench offshore Nicoya Peninsula. The entire incoming sediment section is being underthrust beneath the margin, providing an ideal setting to examine Ba cycling in the shallow levels of the subduction zone. Results from these analyses indicate that a significant amount of Ba is liberated from the mineral barite ($BaSO_4$) in the uppermost hemipelagic sediments arcward of the trench. The shallow distillation of Ba may impact the amount of sedimentary Ba reaching the deeper subduction zone.

INTRODUCTION

Convergent margins are areas of high tectonic activity and dynamic hydrology, making them important regions for geochemical cycling between major reservoirs such as seawater, oceanic sediment and crust, continental crust, and the mantle. The distillation and loss of some volatiles and fluid-soluble elements from the shallow subduction zone changes the composition of the slab (sediments and igneous basement) delivered to the depths of magmatism beneath volcanic arcs and, ultimately, the mantle. The escape of fluids from the downgoing and over-

[1]Solomon, E.A., Kastner, M., and Robertson, G., 2006. Barium cycling at the Costa Rica convergent margin. *In* Morris, J.D., Villinger, H.W., and Klaus, A. (Eds.), *Proc. ODP, Sci. Results,* 205, 1–22 [Online]. Available from World Wide Web: <http://www-odp.tamu.edu/publications/205_SR/VOLUME/CHAPTERS/210.PDF>. [Cited YYYY-MM-DD]
[2]Scripps Institution of Oceanography, University of California San Diego, 9500 Gillman Drive, La Jolla CA 92093-0212, USA. Correspondence author: **esolomon@ucsd.edu**

Initial receipt: 8 March 2005
Acceptance: 22 November 2005
Web publication: 4 April 2006
Ms 205SR-210

riding plates at depth may affect seawater chemistry for select elements and isotope ratios.

Barium is a large-ion lithophile element (LILE) that is incompatible and enriched in oceanic sediments and the continental crust. Ba is strongly partitioned into the fluid phase at moderate to high temperatures and is leached from the oceanic crust at depths of magma generation and incorporated into the melt. As a result, Ba is enriched in arc volcanics worldwide and volcanic outputs reflect the sediment inputs (Morris, 1991; Plank and Langmuir, 1993), assuming there is insignificant loss of Ba with fluids that escape from the downgoing slab. Using bulk sediment input fluxes of Ba and other incompatible elements, coupled with the volcanic output fluxes, the amount of sediment contributed to the arcs as well as the elemental fluxes to the mantle have been estimated (e.g., Plank and Langmuir, 1993; Patino et al., 2000). The incoming sediment section offshore the Nicoya Peninsula of Costa Rica contains 152 m of diatom-rich hemipelagic sediments overlying 226 m of pelagic calcareous nannofossil oozes and chalks. The subducting sediment section offshore Guatemala (Deep Sea Drilling Project [DSDP] Site 495) is nearly identical to that drilled offshore Costa Rica (Fig. **F1**). Ba/La and Ba/Th ratios (Carr et al., 1990; Leeman et al., 1994; Patino et al., 2000), coupled with ^{10}Be isotopic concentrations of the Central American lavas (Tera et al., 1986; Morris et al., 1990, 2002), suggest that the entire sediment section is subducting to depths of magma generation beneath Nicaragua, whereas there is little contribution from the uppermost hemipelagic sediments and a proportionally larger contribution from the pelagic carbonate section at Costa Rica. Since the entire sediment section is subducted at Costa Rica, the low ^{10}Be in the Costa Rican volcanics must be due to sediment dynamics under the forearc, such as sediment underplating or subduction erosion (Morris et al., 2002).

F1. Sediment sections, p. 14.

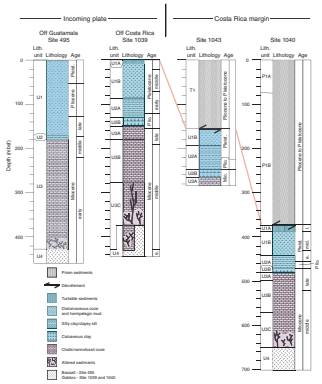

The distribution of Ba in deep-sea sediments is variable. High concentrations are typically found in sediments underlying high-productivity waters (Dymond et al., 1992, 1996; Paytan et al., 1996; Eagle et al., 2003) and are thought to result from the rapid release of dissolved Ba from labile particulate Ba during the early stages of plankton decomposition either by cell lysis or decay of labile organic matter in surface waters (Ganeshram et al., 2003). A fraction of the released Ba precipitates abiotically as barite ($BaSO_4$) within supersaturated microenvironments, where it is deposited on the seafloor (Dehairs et al., 1980; Bishop, 1988; Ganeshram et al., 2003). Ba is also contained in other biogenically related phases such as refractory organic matter and biogenic carbonate, as well as inorganic phases like detrital silicates and Fe-Mn oxides and oxyhydroxides (e.g., Dymond et al., 1992; McManus et al., 1998; Plank and Langmuir, 1998; Eagle et al., 2003). The concentration of these biogenic phases, as well as the detrital phases, may represent a significant fraction of the total Ba in the sediment column, especially at continental margin settings. Ba concentrations are ~600 ppm in Post-Archaean Australian Shale (PAAS) (Taylor and McLennan, 1985) and North American Shale Composite (NASC) (Condie, 1993; Plank and Langmuir, 1998), ~690 ppm in green clay (Plank and Langmuir, 1998), and generally <200 ppm in some volcaniclastic sediments (Elliot et al., 1997; Plank and Langmuir, 1998). In general, sediment samples with total Ba concentrations >1000 ppm contain up to 70% Ba associated with the mineral barite (Eagle et al., 2003).

The Ba in aluminosilicates is typically immobile during sediment diagenesis; however, the Ba in barite is affected by variations in pore fluid

sulfate concentrations (Dymond et al., 1992; McManus et al., 1998; Torres et al., 1996a). In organic-rich sediments, microbial degradation of organic matter leads to sulfate reduction and methanogenesis; the pore water SO_4^{2-} is consumed by oxidation of organic carbon and, at some locations, also by methane oxidation. When pore fluid sulfate becomes depleted, the solubility of barite increases greatly and dissolved Ba^{2+} concentrations can rise by several orders of magnitude (Brumsack and Gieskes, 1983; Torres et al., 1996b; Dickens, 2001). In tectonically active regions, like convergent margins, the dissolved Ba can be transported by compaction-induced fluid expulsion in the underthrust sediments and fluid advection along higher permeability conduits in the décollement and upper fault zones where it is reprecipitated as barite when it reaches SO_4^{2-}-rich water (Torres et al., 2003). Recently, cold seep authigenic barite deposits have been discovered in a wide variety of continental margin environments. Torres et al. (1996a) sampled barite chimneys as high as 15 cm along a scarp failure at the Peru convergent margin. Other deposits have been discovered in the San Clemente Basin (Lonsdale, 1979; Torres et al., 2002), Monterey Bay (Naehr et al., 2000), the Sea of Okhotsk (Greinert et al., 2002), and the Gulf of Mexico (Fu et al., 1994).

Ocean Drilling Program (ODP) Legs 170 and 205 drilled a transect of three boreholes across the Middle America Trench with a reference site seaward of the trench in the incoming sediments and igneous basement (Sites 1039/1253) and two sites landward of the trench that drilled through the margin wedge, the décollement, and the underthrust sediments (Sites 1040/1254 and 1043/1255) (Fig. **F2**). At Sites 1039/1253, sulfate concentrations reach a minimum of ~13 mM within the uppermost 20 m of the hemipelagic sediment section and are near seawater value within the pelagic carbonate section (Kimura, Silver, Blum, et al., 1997) (Fig. **F3C**). At Sites 1040/1254, ~1.6 km landward of the trench, sulfate is totally depleted within the prism sediments and the zero-sulfate zone is also observed in the underthrust hemipelagic sediments to a depth of ~30 m below the décollement (Kimura, Silver, Blum, et al., 1997; Morris, Villinger, Klaus, et al., 2003), despite the fact that minimum SO_4^{2-} concentrations at the reference site were ~13 mM in the uppermost hemipelagic section. This suggests that upon underthrusting, the supply of sulfate from seawater by diffusion ceased and the sulfate reducing bacteria in the underthrust sediments utilized the remaining SO_4^{2-} at the top of the section (Fig. **F3D**). Once this sulfate was depleted, barite would be undersaturated and significant release of dissolved Ba^{2+} would occur. As the incoming sediment section is further underthrust, sulfate depletion would reach deeper levels in the sediment section, further liberating Ba^{2+} from barite. This progressive barite distillation could have a profound impact on the amount of Ba that originally was present within the sedimentary section at Sites 1039/1253 reaching depths of magma generation under the Costa Rican arc volcanoes. This process should operate in all convergent margins and may reduce estimates of Ba input flux to the subduction factory in margins subducting sediments with an appreciable amount of biogenic barite (i.e., bulk sediment Ba > ~1000 ppm).

F2. Seismic profile, p. 15.

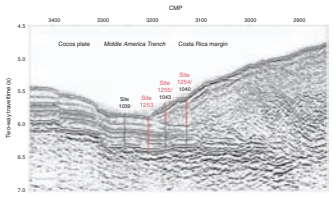

F3. Pore fluid Ba and SO_4 depth profiles, p. 16.

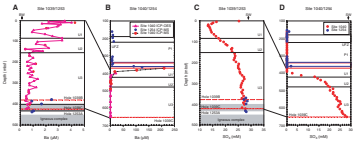

METHODS

Sampling Strategy and Compaction Correction

Both pore fluid and solid samples were measured at Sites 1039/1253 and 1040/1254. Most of the sediment samples were from pore water "squeeze cakes," and intervals with ash layers were not sampled. Since dissolved sulfate is only depleted in lithologic Unit U1 pore fluids at Sites 1040/1254, sampling was at a higher frequency in this unit. Pore fluid samples were analyzed for Ba concentrations by inductively coupled plasma–mass spectrometry (ICP-MS), as well as by inductively coupled plasma–optical emission spectrometry (ICP-OES). All of the sediment samples were analyzed for Ba concentrations by ICP-MS.

In order to correlate sediment samples across holes (from Sites 1039/1253 to 1040/1254), percent compaction estimates for the underthrust sediment based on weight percentage $CaCO_3$ measured shipboard during Leg 170 were employed (Kimura, Silver, Blum, et al., 1997). Assuming that the entire section is underthrust at Costa Rica, the $CaCO_3$ depth profiles from both sites indicate that there was a 36% reduction in thickness of lithologic Unit U1 and Subunit U2A (hemipelagic clayey section), a 62% reduction of thickness of Subunits U2B and U3A (hemipelagic clayey and transition sections), and a 24% reduction of thickness in Subunits U3B and U3C (pelagic calcareous section) (Kimura, Silver, Blum, et al., 1997). These estimates are similar to those presented in Saffer et al. (2000) based on logged bulk density from Leg 170, where the authors estimate a 33% reduction in thickness of the hemipelagic section by Site 1040 and ~20% reduction in thickness of the lower pelagic calcareous section. To correlate the sample depths at Site 1039/1253 to their appropriate depths at Sites 1040/1254, the following equations were used:

$$d_{1040} = (d_{1039} \times \Delta t) + 371 \text{ and} \quad (1)$$

$$d_{1040(n)} = (\Delta d_{1039} \times \Delta t) + d_{1040(n-1)}, \quad (2)$$

where

d_{1040} = corresponding depth at Site 1040,
d_{1039} = depth at Site 1039,
Δt = percent reduction in thickness of each lithologic unit at Sites 1040/1254 determined from the $CaCO_3$ concentration depth profiles at Sites 1039 and 1040,
371 = depth of the base of the décollement at Site 1040,
Δd_{1039} = vertical distance between adjacent samples at Site 1039, and
$d_{1040(n-1)}$ = cross-correlated depth of the previous sample.

Equation 1 is only used for the shallowest sample at Site 1039, and equation 2 is used for all subsequent samples. Compared with the estimates of Saffer et al. (2000), the cross-hole compaction corrected depths in lithologic Units U1 and U2 at Site 1040 would be nearly identical and depths in Unit U3 would be shifted ~15 m deeper as a result of greater compaction in the transition section based on the $CaCO_3$ concentration-depth profiles.

Pore Fluid Analyses

A total of 35 pore fluid samples were analyzed for Ba concentrations on a ThermoQuest/Finnigan Element 2 ICP-MS (see Table T1). All sample and standard preparations were made in a clean laboratory. Samples and standards were diluted with double-distilled deionized water containing 0.4-N HNO_3 and spiked with a 1.0-ppb In internal standard. All standard and calibration solutions were prepared from certified stock solutions. Two unknowns and 20 pore fluid samples were analyzed for each batch of analyses. A 1.0-ppb drift standard was analyzed after every four samples. Blanks were interspersed at random during each batch of analyses, and calibration was achieved with five standard solutions ranging from 0.1 to 5.0 ppb. Pore fluid samples were diluted 100 times at Sites 1039/1253, 1000 times in lithologic Unit P1 at Site 1254, 10,000 times in Unit U1 at Sites 1254/1040, and 100 times in Units U2 and U3 at Site 1040 to achieve a final concentration of ~1.0 ppb, thus matching the concentration of the drift standard and internal standard. Prior to analysis, the ICP-MS was tuned using the ^{115}In internal standard to maximize the intensity of the elements to be analyzed, and mass calibrations were performed after every 20 samples. Instrumental drift was corrected online by normalization of the intensity of the analyte with the intensity of the ^{115}In standard. A second drift correction was applied offline using repeated analyses of the 1.0-ppb Ba drift standard made by dilution of the primary certified stock solution. The accuracy and precision of multiple analyses were monitored by repeated analyses of the two unknowns and the 1.0-ppb drift standard. The average accuracy was <1%, and the average precision was <0.65%.

A total of 65 pore fluid samples were analyzed for Ba concentrations by standard addition on a Perkin Elmer Optima 3000 ICP-OES. The average accuracy and precision of the ICP-OES analyses determined by multiple analyses of drift and calibration standards was <4% and <7%, respectively. The results of the ICP-MS and ICP-OES determinations agree fairly well (Fig. F3) and are within the quoted precision of the ICP-OES analyses. Pore water sulfate concentrations at Sites 1039 and 1040 were measured shipboard during Leg 170 by ion chromatography (IC) using a Dionex DX-100. The reproducibility of the analyses, expressed as 1σ standard deviations of means of multiple determinations of International Association of Physical Sciences of the Ocean (IAPSO) standard seawater was ~1% (Kimura, Silver, Blum, et al., 1997). Sulfate concentrations at Sites 1253 and 1254 were measured shipboard during Leg 205 by IC using a Dionex DX-120. The reproducibility of the analyses, expressed as percent precision from multiple determinations of IAPSO standard seawater was <2%.

Bulk Sediment Chemical Analyses

Sediment samples were dried in an oven for 24 hr at 60°C then ground into a fine powder. The samples were weighed before and after drying to determine the weight of water evaporated. Since the sediment samples were taken from pore water squeeze cakes, Ba concentrations of the pore water splits were used to compute the amount of Ba precipitated as salts during the drying process. Ten milligrams of the powdered sample was weighed and placed in a tightly capped, acid-cleaned polytetrafluoroethylene (PTFE) beaker. All sediment digestions were performed in a clean room. Two U.S. Geological Survey (USGS) certified rock standards were digested with each batch of sediments, typically

T1. Pore fluid Ba, p. 19.

four sediment samples. MAG-1 (marine mud) and SCO-1 (Cody Shale) were chosen as standards because they are marine sediments and have certified values for Ba. The digestion procedure consisted of five steps. Each step included adding an Optima-grade reagent, placing the tightly capped beaker in an ultrasonicator for 60 min, and evaporating to dryness in a PTFE evaporating unit under a heat lamp. The samples were digested by adding 4-N HNO_3 to convert the carbonate to CO_2, adding 30% hydrogen peroxide to oxidize the organic matter, adding a 2:1 mixture of concentrated HF and HNO_3 to digest the sample, and twice treating the samples with concentrated nitric acid. The samples were then diluted 2000-fold by weight with a preprepared 2.5% nitric acid solution in double-distilled deionized water.

All of the sediment samples were analyzed on a ThermoQuest/Finnigan Element 2 ICP-MS. The initial dilution was diluted 500 times by weight to provide a final dilution of 1×10^6 times. All solutions were spiked with a 1.0-ppb In internal standard. The method of analysis by ICP-MS was identical to that performed on the pore fluid samples outlined above. Digestion precision and accuracy were monitored by repeated digestion of reference USGS certified rock standards MAG-1 and SCO-1. Similar final dilutions were made for the sediment standards as the sediment samples. The average percent accuracy and precision of multiple determinations of MAG-1 were <1% and 0.5%, respectively. The average percent accuracy and precision of multiple determinations of SCO-1 were <1.3% and <1%, respectively. A few shipboard X-ray fluorescence (XRF) data analyzed during Leg 170 have been included in Figure **F4** and in the summary section of this report. The samples were measured on an ARL 8420 XRF with reported percent accuracy and precision of 2%–3% (Kimura, Silver, Blum, et al., 1997).

F4. Sediment Ba depth profiles, p. 17.

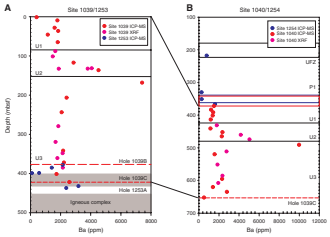

RESULTS

Pore Water

Pore fluid barium concentrations at Sites 1039/1253 and Sites 1040/1254 are presented in Table **T1.** At Site 1039, sulfate concentrations are below seawater value (28.9 mM) at 1.45 meters below seafloor (mbsf) and decrease to a minimum of 13 mM at 24 mbsf (Fig. **F3C**). Sulfate concentrations increase to values seen in surface sediments by 146 mbsf and increase to near-seawater concentration in the basal carbonate section. Ba concentrations are higher than seawater value (~0.15 µM) and variable from 9 to 146 mbsf, which is approximately the base of lithologic Unit U2 (Fig. **F3A**). The dissolved Ba^{2+} concentrations in the upper 146 m of Site 1039 range from 0.378 to 4.257 µM (Table **T1**). Below 146 mbsf, Ba concentrations are nearly constant and slightly above bottom water concentration. Ba concentrations are more variable at Site 1253, at the base of the pelagic carbonate section, due to fluid-rock reactions with the gabbro sill and metalliferous sediments. The Ba concentrations within lithologic Units U1 and U2 at Site 1039 are as much as 26 times seawater value and may be due to Ba mobilization from organic matter as well as Fe-Mn oxides and oxyhydroxides during organic matter diagenesis, as suggested by McManus et al. (1998). The sharp peaks in the Ba profile within these units, as well as in the methane concentration depth profile (Kimura, Silver, Blum, et al., 1997), suggests active lateral fluid advection along coarse-grained ash layers and other more permeable horizons.

The pore fluid within the prism sediments at Sites 1040 and 1254 is totally depleted in dissolved SO_4^{2-} to the base of the décollement at 371 mbsf (Fig. F3D). The zero-sulfate zone is also observed in the uppermost underthrust section to a depth of 401 mbsf. The base of lithologic Unit U1 is at 423 mbsf at Site 1040, and within the other two units, sulfate concentrations gradually increase with depth to a value of 28 mM at the base of the pelagic section (Fig. F3D). The depletion of sulfate in the uppermost hemipelagic sediments at Site 1040 suggests that upon underthrusting the supply of sulfate from seawater by diffusion ceased, and the sulfate-reducing bacteria within the underthrust sediments utilized the remaining SO_4^{2-} at the top of the section. Since the underthrust sediment section is the only source of dissolved SO_4^{2-}, the depth of sulfate depletion will increase arcward. Ba is above seawater value in the prism sediments, and concentrations range from 6.37 to 13.2 µM, indicating some Ba mobilization from barite dissolution. The maximum Ba concentrations within the prism sediments occur within the upper fault zone and the décollement (Table T1), and Ba concentrations are relatively constant at ~6 µM between these two flow conduits. Drilling during Legs 170 and 205 sampled a deeply sourced fluid within these two intervals originating at temperatures as high as ~150°C (Chan and Kastner, 2000; Hensen et al., 2004). Some distillation of Ba at the depth of the deep-sourced fluid may occur.

Most striking are the extremely high Ba concentrations at the base of the décollement in the underthrust sediment section at both Sites 1040 and 1254. The concentrations in lithologic Unit U1 range from 17.26 to 209.57 µM, with the highest concentration occurring at the base of the décollement at 372 mbsf (Fig. F3B). The concentration at 372 mbsf is ~53 times higher than the Ba concentration of the equivalent sample at Site 1039 and ~1400 times higher than the bottom water value. In contrast, the maximum Ba concentration measured within the décollement and upper fault zone at Site 1254 are 9.95 and 13.2 µM, respectively (Table T1). Thus, the extremely high pore fluid Ba^{2+} concentration immediately below the décollement is ~20 times higher than the concentrations measured within the two fluid flow conduits in the prism sediments. The sharp discontinuity in pore fluid Ba^{2+} concentrations between the décollement and uppermost underthrust sediments does not support the suggestion by Saffer and Screaton (2003) that an advective or diffusive flux from the subducted hemipelagic sediments contributes to the Ba signal observed in the décollement and the upper fault zone ~130 m above it, indicating that the two fluid flow systems are effectively decoupled. At 401 mbsf, where SO_4^{2-} concentrations start to increase, Ba concentrations decrease to values similar to those measured at the reference site (Table T1). The extremely high concentrations in the upper 30 m of the hemipelagic section at Site 1040 indicate intense Ba^{2+} liberation from the mineral barite due to increased $BaSO_4$ solubility coupled to SO_4^{2-} depletion. As the subducting sediments move arcward the sulfate depletion zone will become thicker, eventually consuming the pore water SO_4^{2-} in lithologic Units U2 and U3. These units have higher sedimentary Ba concentrations (see discussion below), and a higher proportion of Ba^{2+} will be liberated from barite. This process may have a profound impact on the amount of Ba subducted to depths of magma generation. The diagenetic release and transport seaward of Ba from $BaSO_4$ in sulfate-depleted pore water arcward of the trench may reduce previous estimates of bulk sedimen-

tary Ba subducting to depths of magma generation based solely on the reference section seaward of the trench.

Sediments

Bulk sediment samples were analyzed for Ba to determine if the amount of Ba liberated from barite in the shallow forearc significantly impacts the amount of sedimentary Ba delivered deeper into the subduction zone. The bulk sediment Ba concentration depth profiles for Sites 1039/1253 and 1040/1254 are shown in Figure **F4.** Ba concentrations are the highest at the base of lithologic Unit U2 and in the pelagic carbonate section (Unit U3) where there is less dilution of biogenic Ba by detrital material. Unit U1 and the top of Unit U2 (hemipelagic sediments) have nearly uniform Ba concentrations. The sharp increase in Ba from 2852 to 7408 ppm between 117.53 and 168.45 mbsf (Fig. **F4A**) is caused by a change in sedimentation rate from ~46 to ~6 m/m.y. (Kimura, Silver, Blum, et al., 1997). Most Ba concentrations measured at Site 1039 range from 1000 to 3000 ppm, suggesting that barite is a significant fraction of the Ba-containing phases offshore Costa Rica (Eagle et al., 2003). The Ba concentration-depth profile in the underthrust sediments at Site 1040 is almost identical to that at Site 1039, except concentrations in lithologic Unit U1 are lower than those measured in Unit U1 at Site 1039 (Fig. **F4B;** Table **T2**). Three samples were analyzed for Ba concentrations in the prism sediments at Site 1254. The concentrations are fairly uniform with depth and are 25%–30% of the concentrations measured in the underthrust section, reflecting dilution of biogenic barite by terrigeneous material deposited by debris and gravity flows (Morris, Villinger, Klaus et al., 2003).

Average bulk Ba compositions of each of the lithologic units (Units 1, 2, and 3) at Sites 1039/1253 and 1040/1254 are presented in Table **T3.** The total sedimentary Ba lost or gained across the trench as well as the percent difference in concentration of each unit is also presented in Table **T3.** Unit U1 shows an 18% loss in bulk sedimentary Ba from Site 1039 to Site 1040. Unit U2 displays a 10% loss in Ba, whereas Unit U3 exhibits a 10% gain in Ba between the two sites (Table **T3**). The sampling resolution within Units U2 and U3 is much lower than in Unit U1. Bulk sediment Ba analyses of additional samples within these units are in progress, and results of these measurements will most likely push the percent difference in Units U2 and U3 closer to zero. It is apparent that the percent difference in Unit U1 is almost twice that in Units U2 and U3, indicating that significant Ba distillation due to barite dissolution had occurred and is occurring, effectively changing the bulk Ba composition of Unit U1 as sulfate becomes depleted. As dissolved sulfate becomes further depleted arcward, greater losses of sedimentary barite must exist not only in Unit U1 but in the deeper Units U2 and U3 as well.

Figure **F5** shows cross plots of Ba at Site 1039 vs. Ba at Site 1040 for samples that correlate well across sites. The diagonal line has a slope of 1; therefore, if there were no changes from Site 1039 to Site 1040, then all samples would plot along the 1:1 line. Eighty percent of the samples from lithologic Unit U1 plot well above the line, signifying that the bulk Ba concentrations at Site 1039 are higher than those at Site 1040, whereas samples from Units U2 and U3 plot close to the 1:1 line and are both above and below the line. The pore fluid Ba concentration-depth profile at Site 1040/1254 (Fig. **F3B**) shows the highest dissolved Ba concentrations to occur immediately below the décollement, thus,

T2. Bulk sediment Ba, p. 20.

T3. Lithologic unit Ba compositions, p. 21.

F5. Ba concentrations, p. 18.

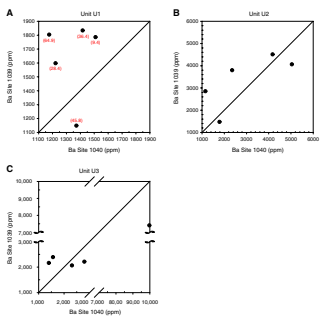

assuming a homogeneous sediment section, one would expect the shallowest samples at Sites 1039/1253 to plot the furthest left of the 1:1 line, which is not observed (Fig. F5A). However, the uppermost hemipelagic sediment section at Sites 1039/1253 is heterogeneous, reflecting varying amounts of detrital material input (Kimura, Silver, Blum, et al., 1997) and differing rates of biogenic barite accumulation with depth, and thus with time. Therefore, Figure F5 does not show a clear trend of the deepest samples in Unit U1 plotting closer to the 1:1 line and the shallowest samples plotting furthest from the line. Results of the sequential barite extraction (in progress) will furnish the absolute barite concentrations of the sediment samples at Sites 1039/1253 and will confirm that each sample in the uppermost hemipelagic sediment section has varying initial barite concentrations and differing amounts of detrital Ba.

CONCLUSIONS AND FUTURE WORK

Bulk sediment Ba concentrations are between 1000 and 10,000 ppm within the underthrust section at Sites 1039/1253 and 1040/1254, indicating that a significant fraction of the sedimentary Ba subducting at Costa Rica is composed of barite. Barite is soluble in regions where pore fluid SO_4^{2-} is depleted. The zone of sulfate depletion extends below the décollement at Site 1040 into the uppermost portion of the hemipelagic sediments. From 371 to 401 mbsf at Site 1040, pore fluid Ba^{2+} concentrations reach 1400 times bottom water value and are ~53 times the concentration of equivalent samples at Site 1039, indicating significant Ba^{2+} liberation from barite within this interval. Comparison of sediment Ba across sites shows that this process influences the bulk Ba concentrations in lithologic Unit U1 at Site 1040. As the sediment section moves arcward, a greater proportion of the underthrust sediment column will be SO_4^{2-} depleted, releasing more Ba from barite. This process may thus have a profound impact on the amount of Ba reaching greater depths in the subduction zone.

The pore fluid Ba^{2+} concentrations measured immediately below the décollement in the uppermost hemipelagic sediments at Site 1040/1254 are ~20 times higher than those measured within the regions of maximum fluid flow in the prism sediments (décollement and upper fault zone). The upper fault zone is situated at ~200 mbsf, whereas the décollement zone extends from ~340 to 371 mbsf at Sites 1040/1254. The décollement and upper fault zone exhibit sharp peaks in lithium, calcium, and C_1–C_3 hydrocarbon concentrations, as well as low chloride and potassium concentrations, indicating advection of a deeper-sourced fluid within these intervals originating at temperatures of ~150°C (Silver et al., 2000; Chan and Kastner, 2000). Though the décollement and upper fault zone are separated by ~130 m, they have nearly identical dissolved Ba^{2+} concentrations that are elevated relative to the pore fluid barium concentrations in the prism sediments between them. The sharp discontinuity in Ba^{2+} concentrations between the décollement and underthrust sediments, but similarity in Ba^{2+} concentrations between the décollement and upper fault zone, ~130 m apart, precludes any significant contribution of barium from the uppermost hemipelagic sediments to the décollement by advective or diffusive flux, indicating that the underthrust sediment and décollement fluid flow systems are effectively decoupled.

Future work will focus on analyzing additional bulk sediment samples for Ba concentrations in Units U2 and U3. A sequential barite extraction procedure using the methods outlined in Paytan (1995) and Eagle and Paytan (2003) is currently being performed on eight sediment samples from Unit U1 at Sites 1039 and 1040 to quantify the absolute change in barite content between the two sites. Once the data set is complete, a more robust average Ba composition of each of the units at both sites and the percent loss of Ba will be computed. Each of the subunits will be weighted and the bulk composition will be computed and used to compute Ba flux to greater depths in the subduction zone following the equations outlined in Plank and Langmuir (1998). Ba loss due to deepening of the sulfate depletion zone arcward will be modeled, and changes to Ba flux rate will be calculated.

ACKNOWLEDGMENTS

This research used samples and/or data provided by the Ocean Drilling Program (ODP). ODP is sponsored by the U.S. National Science Foundation (NSF) and participating countries under management of Joint Oceanographic Institutions (JOI) Inc. This work was funded by JOI-U.S. Science Support Program (USSSP) Grants to E.A. Solomon and M. Kastner. Helpful reviews were provided by Julie Morris and Kristina Faul.

REFERENCES

Bishop, J.K.B., 1988. The barite-opal-organic carbon association in oceanic particulate matter. *Nature* (*London, U. K.*), 332:341–343. **doi:10.1038/332341a0**

Brumsack, H.-J., and Gieskes, J.M., 1983. Interstitial water trace-metal chemistry of laminated sediments from the Gulf of California, Mexico. *Mar. Chem.,* 14:89–106. **doi:10.1016/0304-4203(83)90072-5**

Carr, M.J., Feigenson, M.D., and Bennett, E.A., 1990. Incompatible element and isotopic evidence for tectonic control of source mixing and melt extraction along the Central American arc. *Contrib. Mineral. Petrol.,* 105:369–380.

Chan, L.-H., and Kastner, M., 2000. Lithium isotopic compositions of pore fluids and sediments in the Costa Rica subduction zone: implications for fluid processes and sediment contribution to the arc volcanoes. *Earth Planet. Sci. Lett.,* 183:275–290. **doi:10.1016/S0012-821X(00)00275-2**

Condie, K.C., 1993. Chemical composition and evolution of the upper continental crust: contrasting results from surface samples and shales. *Chem. Geol.*, 104:1–370. **doi:10.1016/0009-2541(93)90140-E**

Dehairs, F., Chesselet, R., and Jedwab, J., 1980. Discrete suspended particles of barite and the barium cycle in the open ocean. *Earth Planet. Sci. Lett.,* 49:528–550.

Dickens, G.R., 2001. Sulfate profiles and barium fronts in sediment on the Blake Ridge: present and past methane fluxes through a large gas hydrate reservoir. *Geochim. Cosmochim. Acta,* 65:529–543. **doi:10.1016/S0016-7037(00)00556-1**

Dymond, J., Suess, E., and Lyle, M., 1992. Barium in deep-sea sediment: a geochemical proxy for paleoproductivity. *Paleoceanography,* 7:163–181.

Dymond, J., and Collier, R., 1996. Particulate barium fluxes and their relationships to biological productivity. *Deep Sea Res. Part II,* 43:1283–1308. **doi:10.1016/0967-0645(96)00011-2**

Eagle, M., Paytan, A., Arrigo, K.R., van Dijken, G., and Murray, R.W., 2003. A comparison between excess barium and barite as indicators of carbon export. *Paleoceanography,* 18(1). **doi:10.1029/2002PA000793**

Elliott, T., Plank, T., Zindler, A., White, W., and Bourdon, B., 1997. Element transport from subducted slab to volcanic front at the Mariana arc, *J. Geophys. Res.,* 102:14991–15019. **doi:10.1029/97JB00788**

Fu, B., Aharon, P., Byerly, G.R., and Roberts, H.H., 1994. Barite chimneys on the Gulf of Mexico slope: initial report on their petrography and geochemistry. *Geo-Mar. Lett.*, 14:81–87. **doi:10.1007/BF01203718**

Ganeshram, R., Francois, R., Commeau, J., and Brown-Leger, S., 2003. An experimental investigation of barite formation in seawater. *Geochim. Cosmochim. Acta,* 67:2599–2605. **doi:10.1016/S0016-7037(03)00164-9**

Greinert, J., Bollwerk, S.M., Derkachev, A., Bohrmann, G., and Suess, E., 2002. Massive barite deposits and carbonate mineralization in the Derugin Basin, Sea of Okhostsk: precipitation processes at cold seep sites. *Earth Planet. Sci. Lett.*, 203:165–180. **doi:10.1016/S0012-821X(02)00830-0**

Hensen, C., Wallman, K., Schmidt, M., Ranero, C.R., and Suess, E., 2004. Fluid expulsion related to mud extrusion off Costa Rica—a window to the subducting slab. *Geology,* 32(3):201–204. **doi:10.1130/G20119.1**

Kimura, G., Silver, E.A., Blum, P., et al., 1997. *Proc. ODP, Init. Repts.,* 170: College Station, TX (Ocean Drilling Program). [**HTML**]

Leeman, W.P., Carr, M.J., and Morris, J.D., 1994. Boron geochemistry of the Central American volcanic arc: constraints on the genesis of subduction-related magmas. *Geochim. Cosmochim. Acta*, 58:149–168. **doi:10.1016/0016-7037(94)90453-7**

Lonsdale, P., 1979. A deep hydrothermal site on a strike-slip fault. *Nature (London, U. K.)*, 281:531–535. **doi:10.1038/281531a0**

McManus, J., Berelson, W.M., Klinkhammer, G.P., Johnson, K.S., Coale, K.H., Anderson, R.F., Kumar, N., Burdige, D.J., Hammond, D.E., Brumsack, H.-J., McCorkle,

D.C., and Rushdi, A., 1998. Geochemistry of barium in marine sediments: implications for its use as a paleoproxy. *Geochim. Cosmochim. Acta,* 62:3453–3473. **doi:10.1016/S0016-7037(98)00248-8**

Morris, J.D., 1991. Applications of cosmogenic ^{10}Be to problems in the earth sciences. *Ann. Rev. Earth Planet Sci. Lett.*, 19:313–350. **doi:10.1146/annurev.ea.19.050191.001525**

Morris, J.D., Leeman, W.P., and Tera, F., 1990. The subducted component in island arc lavas: constraints from Be isotopes and B-Be systematics. *Nature* (*London, U. K.*), 344:31–36.

Morris, J.D., Valentine, R., and Harrison, T., 2002. ^{10}Be imaging of sediment accretion, subduction along the northeast Japan and Costa Rica convergent margins. *Geology,* 30:59–62. **doi:10.1130/0091-7613(2002)030<0059:BIOSAA>2.0.CO;2**

Morris, J.D., Villinger, H.W., Klaus, A., et al., 2003. *Proc. ODP, Init. Repts.,* 205 [CD-ROM]. Available from: Ocean Drilling Program, Texas A&M University, College Station TX 77845-9547, USA. [**HTML**]

Naehr, T.H., Stakes, D.S., and Moore, W.S., 2000. Mass wasting, ephemeral fluid flow, and barite deposition on the California continental margin. *Geology,* 28(4):315–318. **doi:10.1130/0091-7613(2000)028<0315:MWEFFA>2.3.CO;2**

Patino, L.C., Carr, M.J., and Feigenson, M.D., 2000. Local and regional variations in Central American arc lavas controlled by variations in subducted sediment input. *Contrib. Mineral. Petrol.,* 138:265–283. **doi:10.1007/s004100050562**

Paytan, A., 1995. Marine barite, a recorder of oceanic chemistry, productivity, and circulation [Ph.D. thesis]. Scripps Inst. Oceanogr., Univ. Calif. San Diego.

Paytan, A., Kastner, M., and Chavez, F., 1996. Glacial to interglacial fluctuations in productivity in the equatorial Pacific as indicated by marine barite. *Science,* 274:1355–1357. **doi:10.1126/science.274.5291.1355**

Plank, T., and Langmuir, C.H., 1993. Tracing trace elements from sediment input to volcanic output at subduction zones. *Nature* (*London, U. K.*), 362:739–743. **doi:10.1038/362739a0**

Plank, T., and Langmuir, C.H., 1998. The chemical composition of subducting sediment and its consequences for the crust and mantle. *Chem. Geol.,* 145:325–394. **doi:10.1016/S0009-2541(97)00150-2**

Saffer, D.M., and Screaton, E.J., 2003. Fluid flow at the toe of convergent margins: interpretation of sharp pore-water geochemical gradients. *Earth Planet. Sci. Lett.,* 213:261–270. **doi:10.1016/S0012-821X(03)00343-1**

Saffer, D.M., Silver, E.A., Fisher, A.T., Tobin, H., and Moran, K., 2000. Inferred pore pressures at the Costa Rica subduction zone: implications for dewatering processes. *Earth Planet. Sci. Lett.,* 177:193–207. **doi:10.1016/S0012-821X(00)00048-0**

Silver, E., Kastner, M., Fisher, A., Morris, J., McIntosh, K., and Saffer, D., 2000. Fluid flow paths in the Middle America Trench and Costa Rica margin. *Geology,* 28(8):679–682.

Taylor, S.R., and McLennan, S.M., 1985. *The Continental Crust: Its Composition and Evolution:* Oxford (Blackwell Scientific).

Tera, F., Brown, L., Morris, J., Sacks, I.S., Klein, J., and Middleton, R., 1986. Sediment incorporation in island-arc magmas: inferences from ^{10}Be. *Geochim. Cosmochim. Acta,* 50:535–550. **doi:10.1016/0016-7037(86)90103-1**

Torres, M.E., Bohrmann, G., Dube, T.E., and Poole, F.G., 2003. Formation of modern and Paleozoic stratiform barite at cold methane seeps on continental margins. *Geology,* 31(10):897–900. **doi:10.1130/G19652.1**

Torres, M.E., Bohrmann, G., and Suess, E., 1996. Authigenic barites and fluxes of barium associated with fluid seeps in the Peru subduction zones. *Earth Planet. Sci. Lett.,* 170:1–15. **doi:10.1016/S0012-821X(96)00163-X**

Torres, M.E., Brumsack, H.-J., Bohrmann, G., and Emeis, K.C., 1996. Barite fronts in continental margin sediments: a new look at barium remobilization in the zone of sulfate reduction and formation of heavy barites in diagenetic fronts. *Chem. Geol.,* 127:125–139. **doi:10.1016/0009-2541(95)00090-9**

Torres, M.E., McManus, J., and Huh, C.-A., 2002. Fluid seepage along the San Clemente fault scarp: basin-wide impact on barium cycling. *Earth Planet. Sci. Lett.,* 203:181–194. doi:10.1016/S0012-821X(02)00800-2

Figure F1. Incoming sediment sections offshore Guatemala (Site 495) and Costa Rica (Site 1039). The incoming sediment section at Site 1039 is repeated beneath the décollement at Sites 1043 and 1040 arcward of the trench at Costa Rica, suggesting there is no sediment accretion at the toe of the wedge at present (from Morris, Villinger, Klaus, et al., 2003). Stratigraphic column at Site 1253 is nearly identical to that of Site 1039.

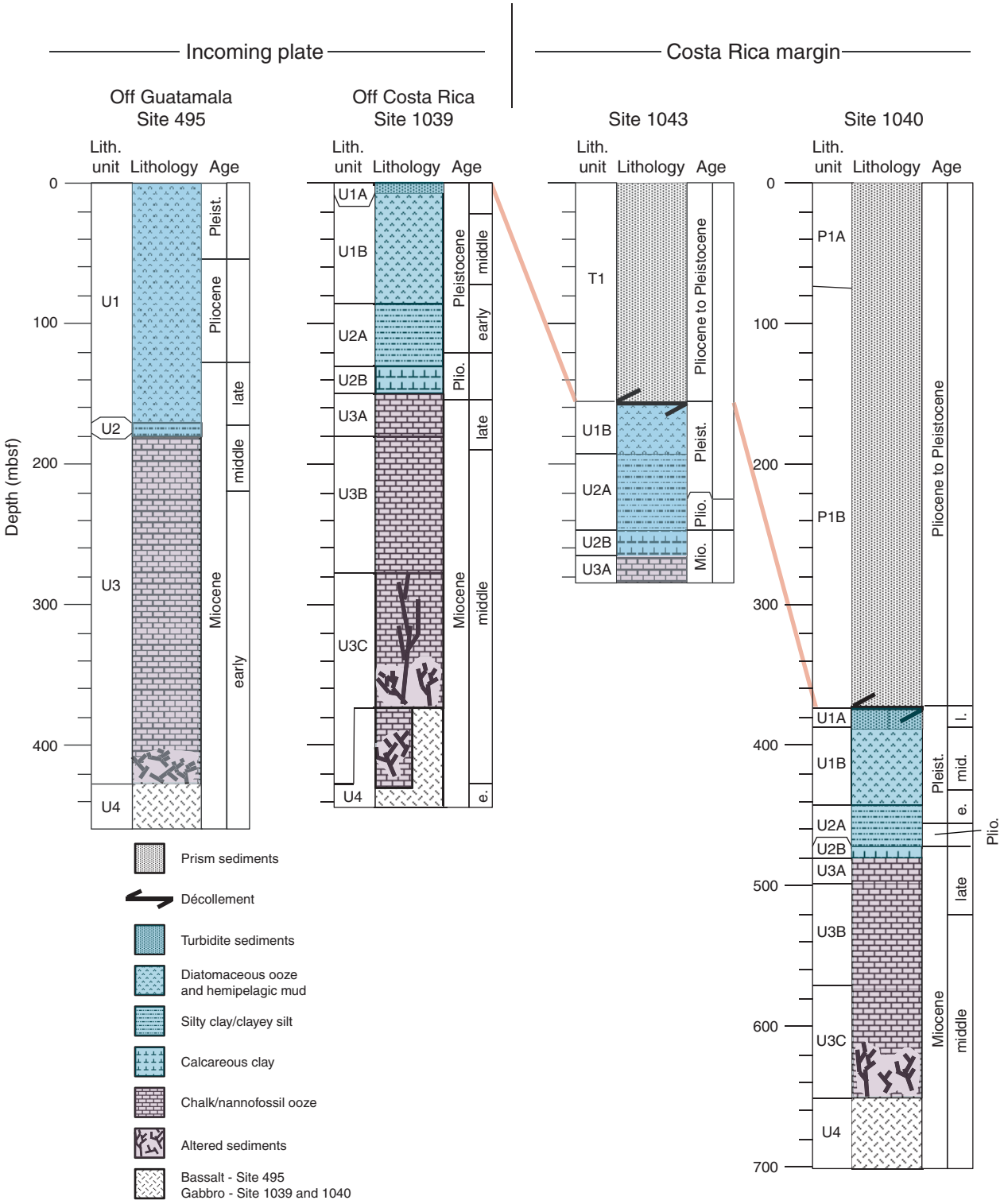

Figure F2. Migrated multichannel seismic Profile BGR-99-44 (Morris, Villinger, Klaus, et al., 2003) across the Middle America Trench. Thick red lines are Leg 205 sites and thin black lines are Leg 170 sites. Site 1253 is ~0.2 km seaward of the deformation front, and Site 1254/1040 is ~1.6 km arcward of the trench. CMP = common midpoint.

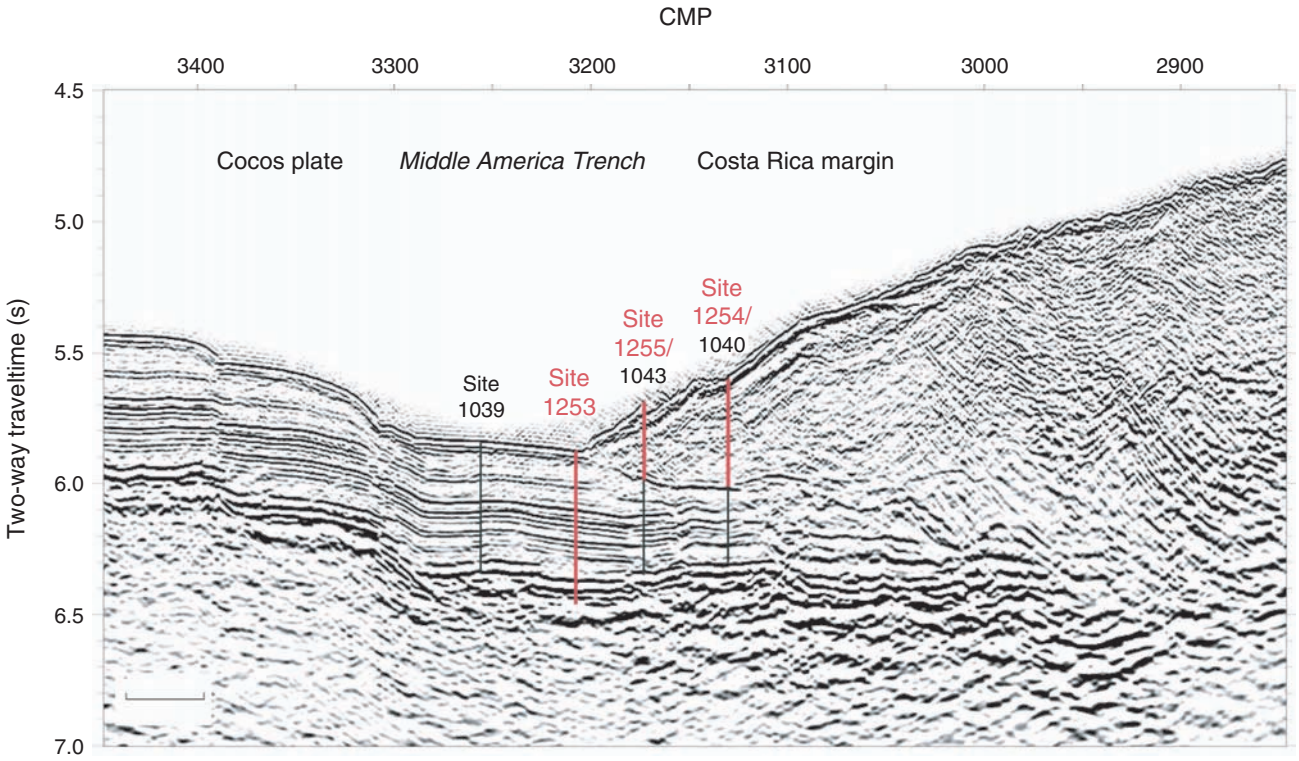

Figure F3. Pore fluid Ba and SO_4 concentration depth profiles along the transect across the Middle America Trench. **A**, **C.** Ba and SO_4 concentrations at Sites 1039/1253. **B**, **D.** Ba and SO_4 concentrations at Sites 1254/1040. Dashed red lines in A and C are the sill depths in Holes 1039B and 1039C. Thin gray shaded area is the sill at Site 1253, and the thick gray shaded area is the igneous complex. Black field in B and D is the upper fault zone (UFZ), the area delineated by blue lines is the décollement at Site 1254, and the area delineated by the solid red lines is the décollement at Site 1040. SO_4 concentrations are from Kimura, Silver, Blum, et al. (1997) and Morris, Villinger, Klaus, et al. (2003). BW = bottom water Ba concentration for the region (Parsons et al. [N1]), SW = seawater, ICP-OES = inductively coupled plasma–optical emission spectrometry, ICP-MS = inductively coupled plasma–mass spectrometry.

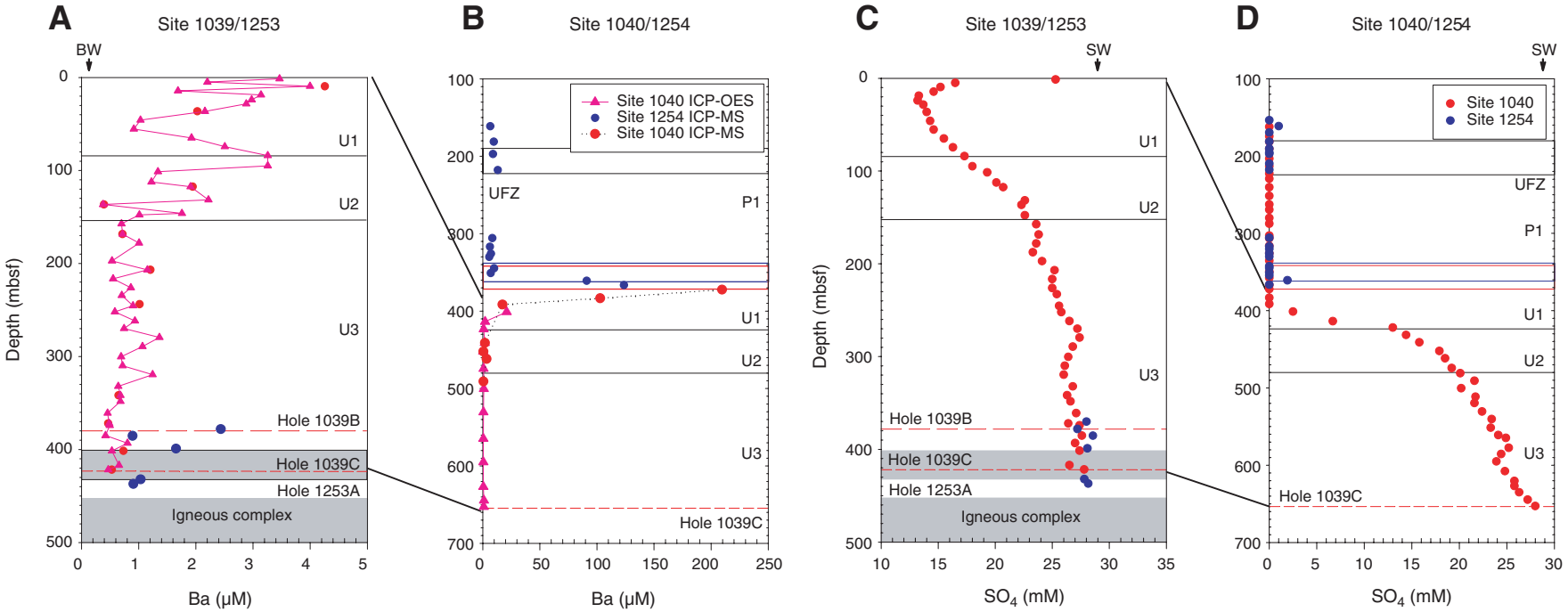

Figure F4. Bulk sediment Ba concentration-depth profiles at (**A**) Sites 1039/1253 and (**B**) Sites 1040/1254. Dashed red lines in A are the sill depths in Holes 1039B and 1039C. The thin gray shaded area is the sill at Site 1253, and the thick gray shaded area is the igneous complex. The black line in B is the upper fault zone (UFZ), the area delineated by blue lines is the décollement at Site 1254, and the area delineated by solid red lines is the décollement at Site 1040. X-ray fluorescence (XRF) data are from Kimura, Silver, Blum, et al. (1997). ICP-MS = inductively coupled plasma–mass spectrometry.

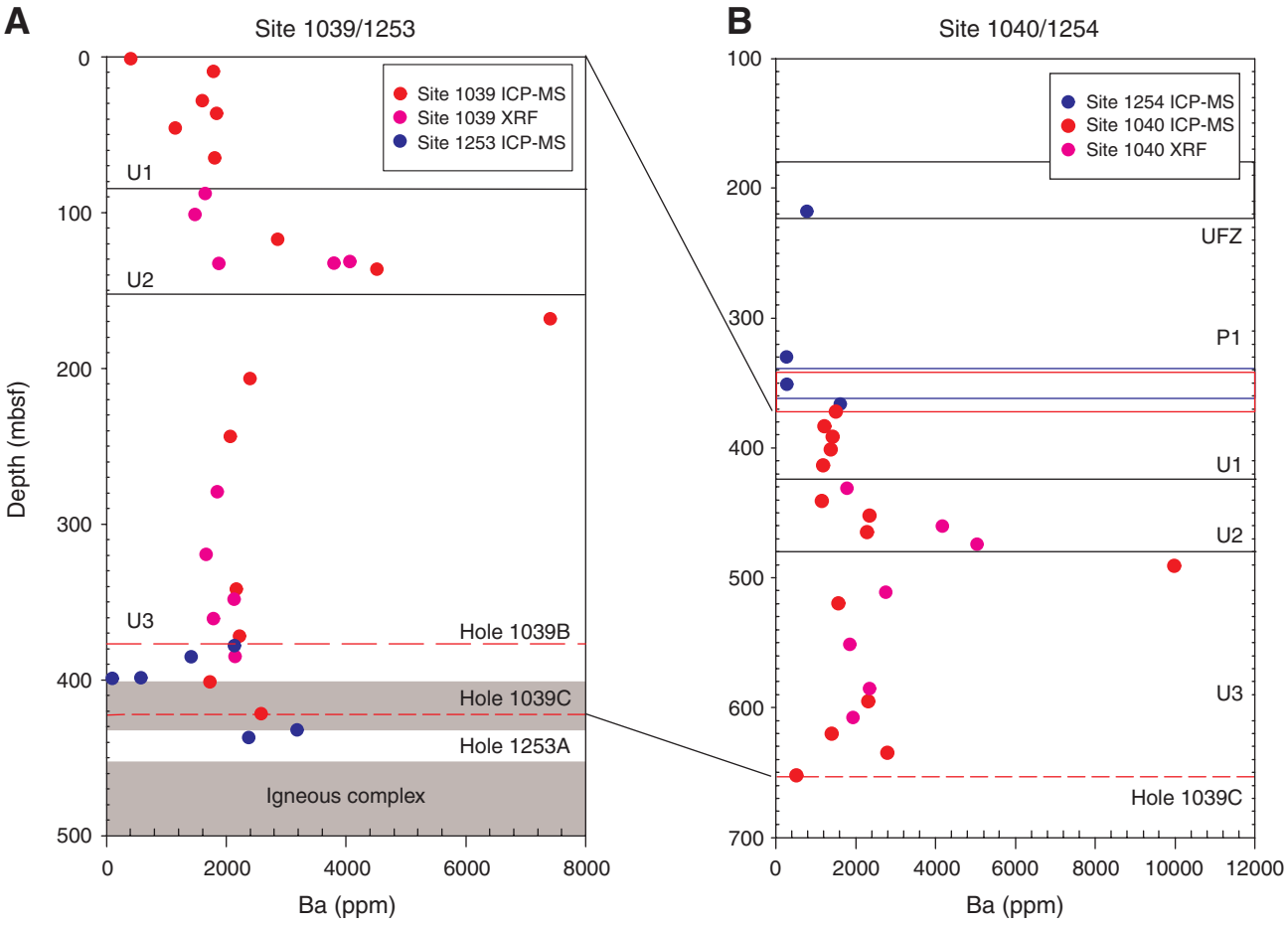

Figure F5. Bulk sediment Ba concentrations at Site 1039 vs. bulk sediment Ba concentrations at Site 1040 for samples that correlate across holes for lithologic (**A**) Unit U1, (**B**) Unit U2, and (**C**) Unit U3. Numbers in parentheses are sample depths in mbsf at Site 1039.

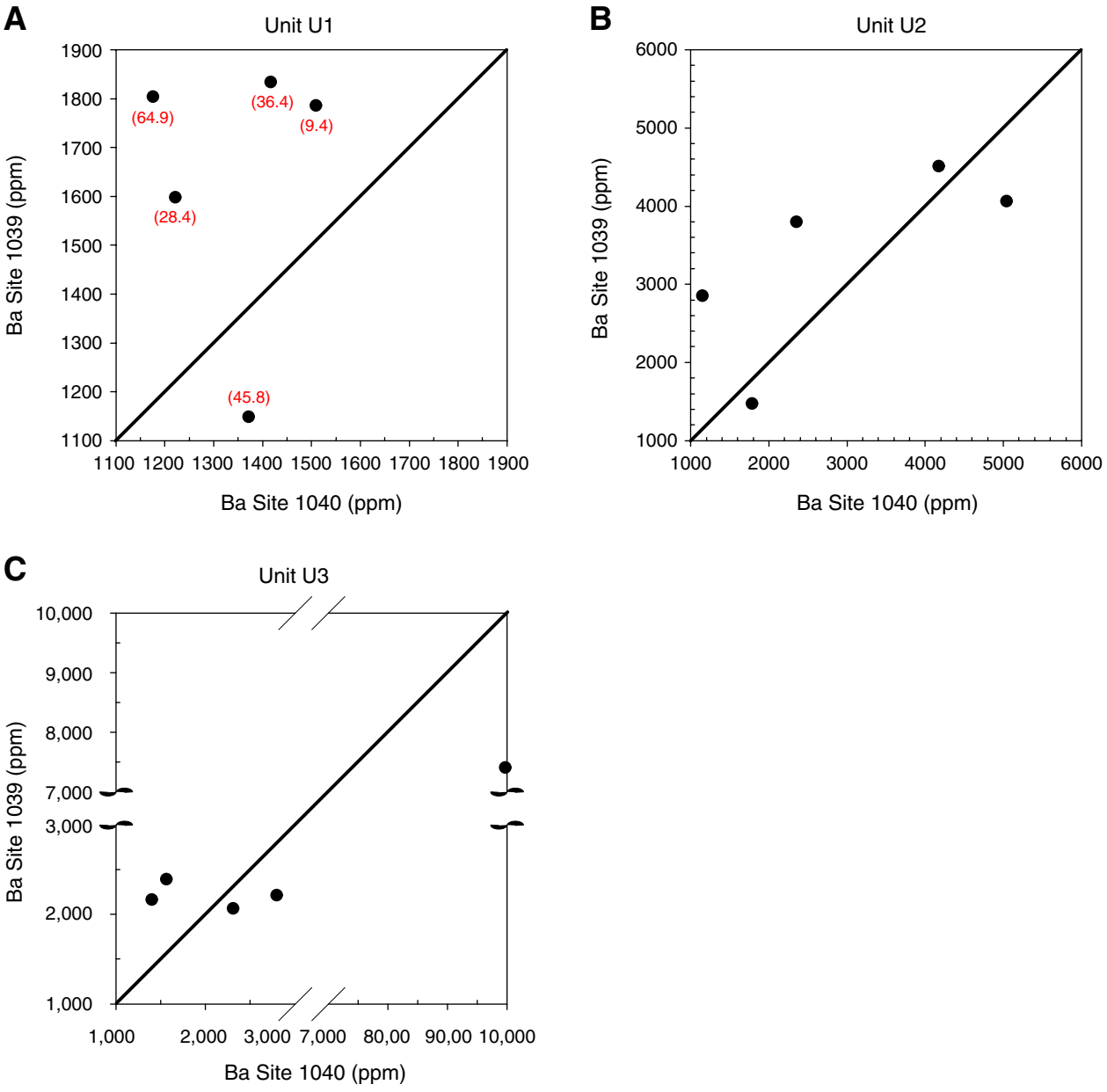

Table T1. Pore fluid Ba concentration data, Sites 1039/1253 and 1040/1254.

Core, section, interval (cm)	Depth (mbsf)	Ba (μM) ICP-MS	Ba (μM) ICP-OES
170-1039B-			
1H-1, 145–150	1.5	—	3.46
2H-2, 140–150	5.0	—	2.20
2H-5, 140–150	9.4	4.26	4.00
3H-2, 140–150	14.4	—	1.69
3H-5, 140–150	18.7	—	3.14
4H-2, 140–150	23.9	—	2.98
4H-5, 140–150	28.4	—	2.88
5H-4, 140–150	36.4	2.03	2.16
6H-4, 134–150	45.8	—	1.03
7H-4, 140–150	55.4	—	0.914
8H-4, 140–150	64.9	—	1.92
9H-4, 140–150	74.4	—	2.51
10H-4, 140–150	83.9	—	3.26
11H-5, 140–150	94.9	—	3.26
12X-3, 135–150	101.4	—	1.34
13X-6, 135–150	112.4	—	1.22
14X-3, 135–150	117.5	1.95	1.91
15X-6, 135–150	131.6	—	2.22
16X-3, 135–150	136.6	0.394	0.378
17X-3, 130–150	146.1	—	1.76
17X-4, 135–150	147.7	—	1.01
18X-4, 135–150	157.3	—	0.700
19X-5, 135–150	168.5	0.717	0.719
20X-5, 135–150	178.0	—	1.01
22X-5, 135–150	197.2	—	0.534
23X-5, 135–150	206.9	1.21	1.15
24X-5, 135–150	216.5	—	0.552
25X-5, 135–150	226.1	—	0.863
26X-4, 135–150	234.3	—	0.704
27X-5, 135–150	245.4	1.02	0.901
28X-3, 135–150	252.1	—	0.584
29X-3, 135–150	261.8	—	0.936
30X-2, 135–150	270.0	—	0.746
31X-3, 130–150	279.5	—	1.36
32X-2, 130–150	289.2	—	1.07
33X-3, 130–150	300.3	—	0.693
34X-3, 130–150	309.9	—	0.718
35X-3, 130–150	319.5	—	1.24
36X-5, 130–150	332.1	—	0.643
37X-5, 130–150	341.7	0.647	0.682
38X-3, 130–150	348.3	—	0.682
39X-5, 130–150	360.9	—	0.458
40X-6, 130–150	372.0	0.467	0.485
41X-1, 130–150	374.1	—	0.492
170-1039C-			
3R-2, 132–150	385.0	—	0.420
4R-1, 132–150	393.2	—	0.803
5R-1, 0–6	401.5	0.734	0.530
6R-4, 128–142	417.0	—	0.656
7R-1, 85–100	421.7	0.530	0.467
205-1253A-			
2R-2, 85–104	378.1	2.44	—
3R-1, 7–23	385.4	0.893	—
4R-3, 100–120	399.0	1.65	—
10R-2, 59–73	432.1	1.03	—
11R-1, 81–96	437.0	0.907	—
205-1254A-			
2R-4, 125–160	161.4	6.67	—
4R-5, 45–90	181.3	9.74	—
6R-2, 125–166	197.2	9.02	—
8R-4, 0–45	217.9	13.21	—
9R-5, 0–45	305.7	8.37	—
10R-6, 0–40	316.9	6.37	—
11R-5, 63–103	325.9	7.26	—
12R-1, 101–141	330.1	5.69	—
13R-5, 69–109	344.9	9.95	—
14R-3, 0–44	351.0	7.01	—
15R-3, 0–44	360.9	91.10	—
16R-3, 49–89	366.4	123.60	—
170-1040C-			
23R-1, 115–150	372.2	209.6	—
24R-2, 120–150	381.8	102.8	—
25R-1, 125–150	391.5	17.3	—
26R-1, 125–150	401.1	—	20.9
27R-3, 125–150	413.7	—	1.99
28R-2, 125–150	423.4	—	0.817
30R-2, 125–150	441.0	1.99	1.80
31R-3, 125–150	452.1	0.578	0.464
32R-3, 125–150	461.8	3.372	—
33R-3, 120–150	474.2	—	0.709
35R-3, 132–150	490.8	0.670	—
36R-3, 135–150	500.4	—	0.943
39R-4, 115–150	530.6	—	0.691
43R-1, 130–150	564.7	—	0.596
46R-2, 130–150	595.1	—	0.548
49R-4, 115–150	626.9	—	0.578
51R-3, 120–140	644.6	—	1.06
52R-2, 125–150	652.8	—	0.961

Notes: ICP-MS = inductively coupled plasma–mass spectrometry, ICP-OES = inductively coupled plasma–optical emission spectrometry. — = sample concentration was not determined by the respective analytical method.

Table T2. Bulk sediment Ba concentration data for representative bulk samples, Sites 1039/1253 and 1040/1254.

Core, section, interval (cm)	Depth (mbsf)	Lithology	Ba (ppm)
170-1039B-			
1H-1, 145–150	1.45	Diatomaceous ooze with interbedded silt, sand	400
2H-5, 140–150	9.45	Diatomaceous ooze with radiolarians	1786
4H-5, 140–150	28.45	Siliceous ooze with minor ash	1598
5H-4, 140–150	36.45	Silty siliceous and diatomaceous ooze	1834
6H-4, 140–150	45.93	Siliceous ooze with minor ash	1148
8H-4, 140–150	64.95	Siliceous ooze with minor ash	1804
14X-3, 135–150	117.53	Silty clay with radiolarians and diatoms	2852
16X-3, 135–150	136.55	Clay with calcareous layers and ash	4512
19X-5, 135–150	168.45	Clayey biogenic ooze	7408
23X-5,135–150	206.85	Nannofossil ooze with diatoms	2394
27X-4, 135–150	243.85	Siliceous nannofossil ooze	2067
37X-5, 130–150	341.7	Siliceous nannofossil ooze	2165
40X-6, 130–150	372	Matrix-supported breccia, biogenic ooze	2216
170-1039C-			
5R-1, 0–6	401.5	Nannofossil ooze with diatoms	1724
7R-1, 85–100	421.65	Diatomaceous nannofossil ooze	2580
205-1253A-			
2R-2, 85–104	378.1	Clay with nannofossils and ash	2134
3R-1, 7–23	385.4	Nannofossil chalk with foraminifers + clay-rich laminations	1413
4R-3, 91–93	398.8	Silicic ash with clay and opaques (big white ash)	572.4
4R-3, 100–120	399	Nannofossil chalk with clay and volcanic ash	93.19
10R-2, 59–73	432.1	Volcanic ash, nannofossils, clay mixed sediment	3180
11R-1, 81–96	437	Claystone with zeolites and spicules	2372
25R-1, 0–3	513.02	Baked sediment claystone with recrystallized calcite	281.24
27R-1, 7.5–9.0	519.34	Baked sediment claystone with recrystallized calcite and quartz	154.08
42R-2, 96–100	592.38	Green clay and zeolite vein	1.98
205-1254A-			
8R-4, 0–45	217.9	Claystone	771.4
12R-1, 101–141	330.1	Calcite-rich claystone	269.07
14R-3, 0–40	351	Claystone with silt, ash, and opaques	277
16R-3, 49–89	366.4	Claystone with ash and diatoms	1614
170-1040C-			
23R-1, 115–150	372.15	Dark olive-green silty clay with diatoms	1509
24R-2, 120–150	383.45	Sandy siltstone with diatoms	1221
25R-1, 125–150	391.58	Olive-green diatomaceous ooze with ash	1417
26R-1, 125–150	401.18	Diatomaceous silty clay	1371
27R-3, 125–150	413.78	Siliceous mudstone with ash	1176
30R-2, 125–150	441.05	Olive-green silty claystone	1147
31R-3, 125–150	452.18	Light grayish green silty claystone with ash	2351
32R-6, 14–17	465.04	Calcareous claystone with diatoms and ash	2284
35R-3, 132–150	490.82	Claystone with vitric ash and diatoms	9971
38R-3, 130–150	519.7	Siliceous nannofossil chalk	1562
46R-2, 130–150	595.2	Green diatomaceous chalk	2309
48R-6, 130–150	620.5	Diatomite with calcareous nannofossils	1397
50R-3, 130–150	635.2	Diatomite with nannofossils and ash	2796
52R-2, 74–80	652.27	Olive-green chalk with accessory zircon	514.1

Table T3. Bulk sediment Ba composition for lithologic Units U1, U2, and U3, Sites 1039/1253 and 1040/1254.

Site	Lithologic unit	Thickness (m)	Average Ba (ppm)	Site	Lithologic unit	Thickness (m)	Average Ba (ppm)	ΔBa (ppm)	ΔBa (%)
1039/1253	U1	84.43	1643.12	1040/1254	U1	51.6	1338.71	–295.42	–18
	U2	68.06	3126.84		U2	57.1	2796.17	–330.67	–10
	U3	268.51	2805.98		U3	173.83	3091.53	+285.54	+10

Note: ΔBa = change in barium concentration from Site 1039/1253 to Site 1040/1254.

CHAPTER NOTE*

N1. Parsons, K.F., Wheat, C.G., Fisher, A.T., Silver, E.A., Underwood, M., and Hutnak, M., submitted. Hydrothermal seepage of altered crustal fluids seaward of the Middle America Trench, offshore Costa Rica. *J. Geophy. Res*.

*Dates reflect file corrections or revisions.